Biogeosciences Discuss., 7, 1057–1099, 2010
www.biogeosciences-discuss.net/7/1057/2010/

Biogeosciences Discussions

This discussion paper is/has been under review for the journal Biogeosciences (BG).
Please refer to the corresponding final paper in BG if available.

A transfer function for the prediction of gas hydrate inventories in marine sediments

M. Marquardt, C. Hensen, E. Piñero, K. Wallmann, and M. Haeckel

Leibniz-Institut für Meereswissenschaften, IFM-GEOMAR, Kiel, Germany

Received: 21 January 2010 – Accepted: 26 January 2010 – Published: 12 February 2010

Correspondence to: M. Marquardt (mmarquardt@ifm-geomar.de)

Published by Copernicus Publications on behalf of the European Geosciences Union.

Abstract

A simple prognostic tool for gas hydrate (GH) quantification in marine sediments is presented based on a diagenetic transport-reaction model approach. One of the most crucial factors for the application of diagenetic models is the accurate formulation of microbial degradation rates of particulate organic carbon (POC) and the coupled biogenic CH_4 formation. Wallmann et al. (2006) suggested a kinetic formulation considering the ageing effects of POC and accumulation of reaction products (CH_4, CO_2) in the pore water. This model is applied to data sets of several ODP sites in order to test its general validity. Based on a thorough parameter analysis considering a wide range of environmental conditions, the POC accumulation rate (POCar in g/cm^2/yr) and the thickness of the gas hydrate stability zone (GHSZ in m) were identified as the most important and independent controls for biogenic GH formation. Hence, depth-integrated GH inventories in marine sediments (GHI in g of CH_4 per cm^2 seafloor area) can be estimated as:

$$\mathrm{GHI} = a \cdot \mathrm{POCar} \cdot \mathrm{GHSZ}^{b} \cdot \exp(-\mathrm{GHSZ}^{c/\mathrm{POCar}}/d) + e$$

with $a = 0.00214$, $b = 1.234$, $c = -3.339$, $d = 0.3148$, $e = -10.265$.

Several tests indicate that the transfer function gives a realistic approximation of the minimum potential GH inventory of low gas flux (LGF) systems. The overall advantage of the presented function is its simplicity compared to complex numerical models: only two easily accessible parameters are needed.

1 Introduction

Since more than two decades, the study of submarine gas hydrates (GH) has attracted increasing interest in the marine geosciences. The reasons for this are, among others: (i) the melting of GH induced by seafloor warming may produce significant greenhouse gas emissions at the seafloor amplifying global climate change in a positive feedback

loop (e.g. Dickens et al., 1995; Kennett et al., 2003; Milkov, 2004). (ii) The dissociation of GH creates overpressures in marine sediments that may trigger slope failure events (Xu and Germanovich, 2006). These mass wasting events may in turn damage cables, pipelines and further facilities for oil and gas production installed on the seabed. (iii) Natural gas bound in GH could become a profitable energy source because of continuously decreasing amounts of conventional fossil fuel resources. Pilot studies aiming at the exploitation of submarine GH are currently carried out in a number of countries (e.g. Japan, India, China, Norway, Germany). Among standard techniques to dissociate GH (i.e. pressure reduction, thermal simulation, and thermodynamic inhibitor injection; Moridis et al., 2004; Sloan and Koh, 2007), a promising new approach of CO_2 exchange for CH_4 is currently investigated (Ersland et al., 2009; Zhou et al., 2008). An improved estimate of mass and distribution of GH stored in marine sediments is a fundamental prerequisite to address these questions.

In general two different main types of marine GH occurrences are distinguished: high gas flux systems (HGF) and low gas flux systems (LGF) (Milkov, 2005). HGF are defined by GH amounts with local concentrations from 5 to up to 100 vol.%. Kastner et al. (2008b) estimated GH concentrations in pore space saturation of up to 67 vol.% for the continental margin of India. Even higher concentrations of 90 vol.% are reported for Nankai by Uchida et al. (2004). Such high concentrations are the result of upward migrating fluids and gases from greater sediment depth which are often enriched in thermogenic CH_4 (Torres et al., 2004; Liu and Flemmings, 2007). From an economical perspective, these are the most interesting areas for future GH-exploitation programs. In contrast, LGF seem to represent the main reservoirs for GH on a global scale. They encompass by far the largest area of active and passive continental margins with average concentrations of about 2 vol.% (Milkov, 2005). Generally, the GH in LGF consists mostly of biogenic CH_4 which is produced within and below the GHSZ. Because of the significantly lower concentrations in LGF, these inventories do not seem to be economically exploitable.

Estimates of the GH inventory

Various geochemical and geophysical methods have been developed and applied to quantify GH-inventories on various scales. However the predictions made since the early 80's vary extremely by several orders of magnitude (Fig. 1). The early estimate of 5.5×10^{21} g of CH_4 stored in the global GH inventory (Dobrynin et al., 1981) has been continuously corrected downward to about 1.4×10^{17} g of CH_4 (Soloviev, 2002) at the turn of the millennium. More recently, there is again a slightly upward trend based on studies by Buffett and Archer (2004), Milkov (2004) and Klauda and Sandler (2005). At present, an inventory of about 4×10^{18} g of CH_4 (3000 Gt C) seems to be the most likely scenario.

Overall, the estimates of the global GH inventory hold discrepancies and inaccuracies of up to five orders of magnitude (Fig. 1). To some extent the mismatch between the different approaches can be explained by the fact that global estimates are based on local or at least regional models, which are then assumed to be representative at the global scale. Such extrapolations depend on a number of more or less constrained parameters which lead to a high level of uncertainty. Typical geophysical approaches to quantify sub-seafloor GH include seismic velocity analysis (e.g. Chand et al., 2004; Westbrook et al., 2008), marine controlled source electromagnetic methods (CSEM; e.g. Chave and Cox, 1982; Schwalenberg et al., 2005), in-situ resistivity measurements (e.g. Kvenvolden, 1988; Yuan et al., 1996; Hyndman et al., 1999), and infrared thermal scanning of sediment cores (e.g. Ford et al., 2003). Estimates based on the geochemical analysis of pore water usually comprise the interpretation of negative Cl^--anomalies as caused by freshwater release during GH dissociation (e.g. Hesse, 2003; Haeckel et al., 2004), and complementary results from pressure core sampling (Heeschen et al., 2007).

In addition, a number of studies (e.g. Davie and Buffett, 2003; Torres et al., 2004; Hensen and Wallmann, 2005; Wallmann et al., 2006) have demonstrated that numerical modelling can be used to constrain rates of GH formation and hence, to predict

GH inventories. The main advantage of transport-reaction models is to constrain rates of GH formation by control parameters such as the particulate organic carbon (POC) input, POC degradation, sedimentation rate, pore water diffusion and advection, heat flow, etc., which can be calibrated against measured pore water and solid phase data. The input and degradation of POC are most critical in this regard as they are the driving force for CH_4 formation (Davie and Buffett, 2001). Several authors used first order kinetic rate laws for modelling the degradation of POC (Davie and Buffett, 2001), based on the assumption that the formation of CH_4 is directly proportional to the availability of incoming POC. Although various approaches have been suggested to describe this process (e.g. Berner, 1980; Westrich and Berner, 1984; Middelburg, 1989), it is still difficult to provide generally valid constraints on the parameterization of these specific rate laws. Moreover, input and composition of organic matter are usually not constant over time (e.g. Berner, 2003), and thus, a generalisation of the POC input and degradation rates may not be appropriate. In some recent models for assessing the global GH inventory (e.g. Buffett and Archer, 2004; Bhatnagar et al., 2007; Archer et al., 2008) rate parameterisations were chosen in a way that a fixed percentage of the POC-flux to the seafloor is converted into CH_4 and GH. In the present study, we test the general validity of a model that uses a second order rate law for POC degradation as suggested by Wallmann et al. (2006) using data from a number of ODP sites. Based on this, we conducted systematic numerical model runs covering a broad range of environmental conditions and geological settings in order to derive a simplified transfer function for the prediction of potential GH inventories.

2 Validation of the numerical model

The transport-reaction model developed by Wallmann et al. (2006) is based on a one-dimensional, numerical approach implemented in Wolfram Mathematica. The model considers steady state compaction of the sediment, diffusive and advective transport of dissolved constituents, input and degradation of POC and particulate organic nitro-

gen (PON) via sulfate reduction and methanogenesis, anaerobic oxidation of methane (AOM), as well as the formation of NH_4, dissolved inorganic carbon (DIC) and CH_4. The model calculates the solubility of CH_4 in pore water, the stability, formation and dissociation of GH as well as the stability, formation and dissolution of free CH_4 gas (FG) in pore water. The general equations and parameterizations of the model are given in the Appendix (Tables A1 and A2); a more detailed description is provided by Wallmann et al. (2006). Specifically, the model calculates the POC-degradation rate as a function of POC input. The rate and reactivity of POC decrease with depth due to age-dependent alteration and inhibition by the accumulation of degradation products (i.e. DIC and CH_4) in the pore water:

$$R_{POC} = \frac{K_C}{C(CH_4) + C(DIC) + K_C} \cdot \left(0.16 \cdot (age_{init} + age_{sed})^{-0.95}\right) \cdot C(POC), \quad (1)$$

where R_{POC} is the degradation rate, K_C is the inhibition coefficient for POC degradation, $C(CH_4)$, $C(DIC)$ and $C(POC)$ are the concentrations of the dissolved and solid species. The central term is an age-dependent term after Middelburg (1989) with age_{init} as the initial age of the POC, and age_{sed} as the alteration time of POC since entering the sediment column.

Specifically the value of K_c is crucial for limiting POC degradation at higher concentrations of CH_4 and DIC. Wallmann et al. (2006) could show that this value seems to be fairly constant (30 to 40 mM) based on results from the Sea of Okhotsk and ODP Site 997 (Blake Ridge). Hence, the major purpose of applying the model to data from various ODP sites is to prove if a generalised parameterisation of POC kinetics is feasible to receive good fits to data from diverse geological environments. Therefore, the model was applied to data from ODP Site 1041 (Costa Rica), Sites 685 and 1230 (Peru), Site 1233 (Chile), Site 1014 (California), Site 995 (Blake Ridge), and Site 1084 (Namibia). GH were previously recovered and/or confirmed at ODP Sites 1041, 685, 1230 and 995. All required environmental information comprising e.g. water depth (hydrostatic pressure), geothermal properties (heat flow), seafloor temperature and sedimentation rate for each site was obtained from the respective ODP reports (D'Hondt et al., 2003;

Kimura et al., 1997; Mix et al., 2003; Paull et al., 1996; Suess et al., 1988; Westbrook et al., 1994) and is summarised in Table 1. Overall, sedimentary strata between 200 and 800 mbsf were recovered from these sites. At Site 1041 the bottom of the stability zone (BSZ) is not reached within the sedimentary deposits. In general, the overall POC concentrations are high (>0.5 wt.%) and the SO_4-penetration depth is low and accompanied by a strong increase of sub-surface NH_4- and CH_4-levels.

Each of the standard models was run into steady state by fitting the model to concentration-depth profiles of the dissolved species SO_4 and NH_4 and the solid species POC and PON. Standard runs consider constant POC input over time as well as sediment burial and molecular diffusion as the only transport processes (a-model run runs). Additional runs with variable POC input (b-model runs) and fluid advection (c-model runs) were performed as specified below (Table 1) in order to comply with site-specific conditions.

All model results (including predicted GH volumes) and measured concentrations of SO_4, NH_4, POC, and PON (if available) are shown in Figs. 2–7. The boundary concentrations used in this study are listed in Table A2 of the Appendix. For all models the concentrations at the upper boundary of the dissolved species SO_4, CH_4 and NH_4 have been prescribed to fixed values corresponding to standard seawater composition (Dirichlet conditions). At the lower boundary zero-gradient conditions are chosen for the a- and b-models (Neumann conditions). For the c-models, which consider advective fluid flow from below, the concentrations of the dissolved species have been determined as Dirichlet conditions. Therefore, the SO_4- and NH_4-concentrations at the lower boundary were set to zero and CH_4-concentration was taken from the output of the respective a-model. The input of POC at the upper boundary is given by a fixed concentration, which is modulated into a time-dependent function considering variations in the POC input over time for the b-models:

$$\mathrm{POC}(x = 0) = f(t) \tag{2}$$

The PON input was determined by fitting the N/C ratio to the respective POC-PON-data at each site.

Pore water SO_4 and NH_4 are the most important parameters for fitting the model. POC and PON usually show more natural variability, and hence are more difficult to constrain. At the depth where CH_4-saturation with respect to methane hydrate is reached (calculated after Tishchenko et al., 2005) GH starts to precipitate. Average GH concentrations without considering fluid flow are generally below 1% of the pore volume (Figs. 2–7). These comparatively low concentrations are in agreement with recent studies at locations which are not affected by intense fluid or gas flow (Milkov, 2005; Tréhu et al., 2004).

2.1 Site-specific results

2.1.1 Costa Rica

Site 1041 is located at the active, erosive continental margin of Costa Rica at a water depth of about 3300 m. Measured data at this location can be sufficiently represented by the standard model (Fig. 2). However, POC and PON data indicate considerable variations in the input of organic material over time. In order to evaluate to which extent such variations may affect GH inventories a second run was performed where the POC input at the sediment surface was varied over time. The result is a better fit to POC and PON data, which, however, only affects estimated GH concentrations by about 20%. Slight deviations from the measured NH_4 profile in both runs may be explained by lateral advection of fluids (Hensen and Wallmann, 2005), which may explain local GH occurrences between 115 and 165 mbsf at this site (Kimura et al., 1997). However, since this process is probably of minor importance and also very difficult to constrain, it will not be further addressed in this study.

2.1.2 Peru

The ODP Sites 1230 and 685 are located on the lower slope of the Peru margin at about 5000 m water depth (D'Hondt et al., 2003). Both sedimentary sequences are

part of the accretionary wedge that forms due to subduction of the Nazca plate. At Site 1230, SO_4 and NH_4 profiles are well reproduced by the standard model (Fig. 3). An average of the measured POC concentrations was used as the POC input value in order to comply with the considerable scatter observed in the depth profile. The GH content is 0.64 vol.% on average and extends from about 60 to 260 mbsf, which excellently matches with the depth interval reported for GH findings (D'Hondt et al., 2003). However, the sedimentary sequence recovered at the nearby Site 685 is considerably thicker (620 m) and indicates that NH_4 decreases with depth (Fig. 3). A model run without fluid flow results in a NH_4-profile which is not supported by the data, but reveals GH concentrations purely based on in situ degradation rates (Fig. 3). Average GH inventories in the no-flow scenarios are approximately the same at both locations, and hence give a good approximation of minimum GH inventories. Based on drilling results (D'Hondt et al., 2003) and similar to findings offshore Costa Rica (Hensen and Wallmann, 2005), upward advection of deep-seated NH_4-depleted fluids is a likely explanation for the observed decrease in NH_4. In a second model run, we applied an upward advection rate of 0.16 mm yr^{-1} and varied the model parameterisation accordingly in order to fit the model to the NH_4 data (Table 1). In agreement with previous studies (Buffett and Archer, 2004; Hensen and Wallmann, 2005) GH inventories in this scenario increase significantly from 26 g of CH_4/cm^2 (a-model) to 66 g of CH_4/cm^2 (c-model).

2.1.3 Southern Chile

Site 1233 is located in a small forearc basin on the upper continental margin (840 mbsf) offshore Southern Chile, belonging to the southern end of the Nazca subduction system. The area is characterised by very high sedimentation rates of about 100 cm/kyr. The standard model does not produce a good fit to the data and does not predict any formation of GH (Fig. 4). The mismatch is obviously caused by changes in the POC input over time and, considering the down-core decrease of NH_4, most likely fluid advection. Increasing the POC input over the past 20 000 years (derived from the

POC-data and the sedimentation rate), however, improved the fit to the data, but did not change the result with respect to GH accumulation. Additional consideration of fluid flow results in a good fit to the data (c-model in Fig. 4) and predicts the presence of minor amounts of GH between 60 and 80 mbsf. All in all, the in situ production of CH_4 is most likely not sufficient to produce GH at this site.

2.1.4 California

Site 1014 was drilled in the Tanner Basin, which belongs to the band of California Borderland basins and is characterised by high organic matter input and an extended oxygen minimum zone between 500 and 1500 m water depth. The standard model revealed a good fit to the measured data (Fig. 5). However, the scatter in the POC input over time was not resolved in the a-run. An average input value of 5 wt.% of POC produced an excellent fit to the measured NH_4 profile, and hence is obviously a good approximation of the overall POC degradation. In spite of the high POC accumulation, GH are not reported for this site. Most likely this is due to the high geothermal gradient of 58°/km resulting in a thin GHSZ. The model predicts minor amounts of GH at the BSZ.

2.1.5 Blake Ridge

The Blake Ridge ODP Site 995, which was drilled into a large drift deposit located at the passive continental margin of the south-eastern United States, has been studied in detail with respect to GH in the past (e.g. Dickens et al., 1997; Egeberg and Dickens, 1999). Using a constant POC and PON input in the basic a-model run does not comply with the measured data and did not predict any GH formation (Fig. 6). In addition, a very high initial sediment age of 180 kyr had to be used in order to achieve POC degradation rates that enable a good fit to the measured NH_4 profile. Using a reduced POC/PON input for the Late Quaternary (Paull et al., 2000) required higher overall degradation rates in order to fit the NH_4 data and predicted GH formation in the depth

range reported previously (Paull et al., 1996). Moreover, Wallmann et al. (2006) used the same model approach as in the present study and predicted roughly the same amount of in situ GH formation for the nearby ODP Site 997. However, overall GH inventories may be still higher due to upward migration of free gas, which is formed below the BSZ (Wallmann et al., 2006).

2.1.6 Namibia

Site 1084 is located on the upper continental margin off Namibia, a region which is characterised by intense upwelling and enhanced POC deposition. Likewise, average POC concentration of >5 wt.% are observed throughout the entire core resulting in high degradation and GH formation rates. Similar to Sites 685 and 1233 (Figs. 3 and 4) the NH_4 profile indicates upward fluid advection at this location. Applying fluid advection to the model leads to a better fit of the NH_4 profile and predicts about 60% higher GH amounts (Fig. 7).

The results above clearly demonstrate the general validity of the kinetic model. The model is able to reproduce the concentrations of solid and dissolved species of the ODP Sites in a generalised way, while all parameters of the kinetic rate law (Eq. 1, Table 1) are kept almost constant. Hence, the model serves as a useful basis for a systematic analysis of biogenic GH formation and the derivation of an analytical transfer function to predict submarine GH inventories. Overall, GH concentrations resulting from all model runs at the ODP Sites without fluid flow vary between 0 and 26 g of CH_4/cm^2 (0 to 1.6 vol.%). In some cases, fitting the NH_4 profiles required the implementation of upward fluid flow, which increases the GH amount up to 66 g of CH_4/cm^2 (~2.2 vol.%; Table 3). Although very significant in terms of GH formation, fluid flow is very difficult to constrain and predict on regional to global scales, and hence was neglected in the following systematic analysis. Consequently, all results presented here have to be regarded as minimum estimates, which only reflect pure biogenic methane and GH formation within the GHSZ.

3 Sensitivity analysis of the standardised numerical model

In order to identify the most important parameters, which significantly control the formation of GH, a sensitivity analysis was performed with parameter variations covering a wide range of natural environments. This analysis is based on a standardised model set up (Table 2), which is defined by the average values of the environmental and chemical conditions (i.e. water depth, thermal conditions, POC concentration, POC initial age (age_{init}), C/N ratio, porosity, sedimentation rate, inhibition constant of POC degradation (K_C), NH_4 adsorption coefficient) of the ODP models (Table 1). Critical parameters for generalization purposes are the age_{init} and K_C since they may have a substantial effect on GH formation rates. In general, high K_C- and low age_{init}-values favour higher degradation rates of organic matter, going along with enhanced formation of NH_4, CH_4, GH, a shallow sulphate penetration depth, and vice versa. A sensitivity analysis of age_{init} confirms that the accumulation of GH generally increases with decreasing initial POC ages (Fig. 8). The effects are strong at high sedimentation rates and comparably small in slowly accumulating sediments. Most of the age_{init} values applied in the ODP models are about 40–50 kyr, with a few exceptions to higher (a- and b-model of Site 1041 and a-model of Site 995) and lower initial ages (Site 1233), and hence an average value of all ODP models (43.7 kyr) was used in the standard model. The average K_C value in the ODP model runs is 43 mM with a quite narrow range of 25 to 50 mM, which is in agreement with results of Wallmann et al. (2006).

Subsequently, the effect on the GH formation was analysed by varying water depth, thermal conditions, sedimentation rate, and POC concentration of the standard model. In these scenarios, the thermal gradient ranges from 10 to 65°/km, the seafloor temperature from 1 to 6°C, and the water depth from 500 to 6000 m. The total sediment thickness was always chosen to be thick enough to include the entire GHSZ. The POC input concentration has been varied from 0.5 to 5.5 wt.%. The sedimentation rate ranges from 10 to 200 cm/kyr. All parameter variations are listed in Table 2.

In Fig. 9 the relation between the tested parameters and the calculated GH amount

BGD
7, 1057–1099, 2010

is summarised. The amount or inventory of gas hydrates (GHI in g of CH_4/cm^2) is calculated by integrating the hydrate concentrations in each layer over the entire model column. The seafloor temperature and the thermal gradient show a negative correlation with GHI because higher temperatures reduce the extension of the GH stability field. Similarly, the GHSZ thickens with increasing water depth because of increasing environmental pressure. Overall, a thick GHSZ causes a longer residence time of POC, and hence favours the formation of biogenic CH_4 within it. The sole effect of the sedimentation rate on the GH formation is comparatively low. For sedimentation rates up to 75 cm/kyr there is a positive correlation with GHI (up to 2.6 g of CH_4/cm^2) because of increasing burial of POC. However, as discovered previously by Davie and Buffett (2001), further increasing sedimentation rates (without increasing POC at the sediment surface) lead to decreasing GH inventories; this transition into a negative trend when reaching a critical maximum is due to the reduced residence time of the degradable POC within the GHSZ, and hence limits the enrichment of CH_4 and GH. Interestingly, the sulphate methane transition (SMT) shows no clear relationship to GH formation. The SMT is affected by the methane flux from below and the sulphate reduction occurring in the uppermost sediment layers. Hence, high rates of POC degradation at shallow depth will consume much of the sulphate, but simultaneously reduce the potential of methane formation at greater depth. While Dickens and Schneider (2009) and Bhatnagar et al. (2008) use the SMT as a proxy to determine recent GH concentrations in the sediment, our results supports the hypothesis of Kastner et al. (2008a) that the SMT is not a good measure for hydrate accumulation in the underlying sediment sequence. The other tested parameters display clear functional relationships to the calculated GH concentration (Fig. 9). However, for the derivation of a simple and useful transfer function it is crucial to limit the set of parameters to those which have (i) a strong effect on the formation of GH and (ii) are widely available and easy to determine. Moreover, the sensitivity analysis above suffers from a lack of systematics; e.g. POC concentration and sedimentation rate or water depth and bottom water temperature have been treated as independent parameters although they are generally correlated.

Hence, in order to perform a refined and more robust analysis, we summarised the parameters defining the temperature and pressure conditions (water depth, thermal gradient and sediment surface temperature) into one parameter which then defines the thickness of the GHSZ (in the following just GHSZ). In addition, the general correlation between POC concentration and sedimentation rate (Henrichs, 1992; Tromp et al., 1995; Burdige, 2007) was accounted for by combining these parameters into the POC accumulation rate (POCar). Since all other parameters are either intrinsically considered (because they are not independent), such as the SMT or the POC degradation rate, or may have only a minor additional effect on GH formation, such as the porosity, they have been excluded from the subsequent analysis.

4 Derivation of the transfer function

In a second and more detailed parameter analysis the effect of POCar and GHSZ was analysed in a number of runs of the standardised numerical model by covering a wider range of natural variations of these parameters than in typical continental margin environments: GHSZ from 100 to 2000 m (Dickens, 2001) and POCar from 0.8 to 40 g/cm^2/yr (Seiter et al., 2005). The GHSZ was varied by changing the thermal gradient from 10 to 65°/km, the seafloor temperature from 1 to 6 °C, and the water depth from 500 to 6000 m. In order to identify possible interdependencies between POCar and GHSZ, crosswise variations were calculated. Because the POCar is defined by the POC concentration and the sedimentation rate, the input concentration of POC was derived by an analytical function of the sedimentation rate based on data from Seiter et al. (2004) and Colman and Holland (2000) (Fig. 10). Although the plot reflects a large range of natural variations of POC concentrations at the sediment surface (average of the upper 10 cm), POC shows a general correlation with the sedimentation rate, which can be expressed by:

$$\mathrm{POC} = -2.8 \cdot \exp(-44.5 \cdot \omega) + 3.0 \quad (3)$$

where POC is in wt.% and ω is the sedimentation rate in cm/yr. Equation (3) was applied for sedimentation rates between 10 to 200 cm/kyr, which corresponds to POC contents between 1.2 to 3.1 wt.% and POCar variations between 0.8 to 37.4 g/m^2/yr.

The functional relationship between the GHSZ and GHI is shown in Fig. 11a. Generally, the plot shows that at constant POCar the amount of GH increases with the thickening of the GHSZ, because of the longer residence time of the degradable material within a thicker GHSZ. Higher POCar causes more GH being formed in the sediment and the gradient of the GH formation increases for higher POCar. It is remarkable that GHI increases only for POCar up to 10 or 15 g/cm^2/yr. The gradient decreases again for POCar >15 g/cm^2/yr (dark blue and black lines in Fig. 11a), most likely because for such high POCar (sedimentation rates >70–100 cm/kyr) the residence time of organic matter within the GHSZ decreases significantly.

In general, higher POCar leads to a higher POC degradation rate and therefore to enhanced formation and saturation of CH_4 in the pore water (Fig. 11b), which has been observed in numerous studies before (e.g. Wallmann et al., 2006; Malinverno et al., 2008). Similar to the test of the sedimentation rate (Fig. 9) and analogous to Fig. 11a, the amount of GH decreases after reaching a critical maximum in POCar of 10 to 15 g/cm^2/yr. The decrease of the GH concentration after reaching this maximum is considerably stronger at a GHSZ of 1353 m compared to a thinner GHSZ of 376 m. Overall, GH inventories increase to higher values with a thicker GHSZ (e.g. at a POCar of 15 g/m^2/yr, 115 g of CH_4/cm^2 for a GHSZ of 1353 m compared to 10 g of CH_4/cm^2 for a GHSZ of 376 m).

The cross-plots of both parameters indicate minimum values of POCar and GHSZ, which are required to form GH. If the GHSZ is too thin, the residence time of POC within the GHSZ is too short for sufficient degradation, and consequently the saturation level of dissolved CH_4 to produce GH will not be reached. The figure also indicates the minimum thickness of the GHSZ to form GH, e.g. this is 500 m at POCar of 2 g/m^2/yr or 250 m at POCar of 6 g/m^2/yr. Overall the model implies that hydrates may form only when the GHSZ exceeds 150 to 200 m (Fig. 11a). This result is in good agreement

with the general depth of the BSR at LGF on the upper continental margins of >200 m (e.g. 240 mbsf on the northern Cascadia margin; Riedel et al., 2006; 200 mbsf on the Svalbard margin; Hustoft et al., 2009). However, GH can still be formed at a lower thickness of the GHSZ if fluid flow and/or gas ebullition are involved (e.g. Torres et al., 2004; Haeckel et al., 2004). Likewise minimum values can also be derived for POCar. As outlined before, if the input of POC is too small due to lower sedimentation rates, most of the POC is degraded by sulphate reduction, and hence only little or no GH can form. Figure 11b shows that a POCar of ~0.8 g/m^2/yr (corresponding to a SR of 10 cm/kyr and an initial POC concentration of 1.2 wt.%) is a threshold value, below which CH_4 can not be sufficiently enriched in most continental margin settings featuring a GHSZ of less than 1200 m).

Each of the model series indicated in Fig. 11 can be fitted by the following two types of equations: The GHSZ-GH relation (Fig. 11a) is best expressed by a potential function of the general form:

$$\mathrm{GHI} = (s \cdot \mathrm{GHSZ}^{u}), \quad (4)$$

where GHI is the depth-integrated inventory of GH [g CH_4/cm^2]. GHSZ is in m. The POCar-GHI relation (Fig. 11b) is approximated by a Maxwell-type equation of the form:

$$\mathrm{GHI} = v \cdot \mathrm{POCar} \cdot \exp(-w^{x/\mathrm{POCar}}/y) + z \quad (5)$$

The differences between the fit-functions in both series of runs are caused by variation of the coefficients s, u, v, w, x, y and z. The choice of coefficients depends on GHSZ (Eq. 4, Fig. 11a) and POCar (Eq. 5, Fig. 11b).

For the derivation of a general transfer function of POCar and GHSZ, Eqs. (4) and (5) were combined by including the GHSZ-term (Eq. 4) into Eq. (5) in order to ensure that the gradients increase with increasing GHSZ and to consider the decrease of GH concentrations beyond a threshold value of POCar (Fig. 11b). A second GHSZ-term was included in the exponent to reproduce the shift of the GH maximum for thicker GHSZ. The constants were determined using the method of least squares for all data

resulting from the parameter analysis. The resulting transfer function is (solid lines in Fig. 11):

$$\mathrm{GHI} = a \cdot \mathrm{POCar} \cdot \mathrm{GHSZ}^{b} \cdot \exp(-\mathrm{GHSZ}^{c \cdot / \mathrm{POCar}} / d) + e, \quad (6)$$

with $a = 0.00214$, $b = 1.234$, $c = -3.339$, $d = 0.3148$, $e = -10.265$.

GHI is the depth-integrated GH inventory in [g of CH_4/cm^2], POCar is the accumulation rate of POC in [g/m^2/yr], and GHSZ is the thickness of the GH stability zone in [m]. Negative GHI values generated by the transfer function indicate the absence of gas hydrates in the considered sediment column.

5 Test and application of the transfer function

To perform a preliminary test and verification of the accuracy of the transfer function (Eq. 6) we calculated the GH content for all parameterizations of the model runs of the sensitivity and the parameter analyses. The transfer function reproduces the modelled data quite well; most data points plot along the 1:1 correlation line (Fig. 12). The general scatter is moderate, however, it is more pronounced at lower concentrations, where errors of more than 50% occur. Overall, the standard deviation (σ) of the function is 8.5 g of CH_4/cm^2 and the correlation coefficient (r) is 0.99.

In addition, the function has been applied to the ODP Sites of Costa Rica, Peru, Chile, California, Blake Ridge and Namibia, which are presented in Sect. 2. The results are listed in Table 3. The GH amounts calculated with the transfer function are all between 0 and 25 g of CH_4/cm^2 and are consistent with the results of the ODP-Site models without the additional upward fluid flow. Additionally, the validity of the transfer function was tested by comparing its results with several published studies based on direct observations, geochemical modelling and other methods (resistivity logs, chlorinity anomalies, and seismic velocity analysis; Table 4). Overall, the GH concentrations obtained with the transfer function are in good accordance with the results of several modelling studies in LGF systems, such as the northern Cascadia margin

(ODP Leg 311) or Blake Ridge (Table 4). The transfer function does not predict any GH for Hydrate Ridge, which is in line with results of Torres et al. (2004) and Tréhu et al. (2004) who state that strong GH enrichments at the summit (Sites 1249–1250) are due to enhanced gas flux. Away from the summit (Sites 1244–1248) there is almost no indication for GH formation.

Kastner et al. (2008b) estimated GH concentrations from 8 to 495 g of CH_4/cm^2 (1 to 61 vol.%) at the Indian continental margin (Site 10). Assuming that the lower concentrations display the regional background concentration of GH, the amount calculated by the transfer function of 5.4 g of CH_4/cm^2 is in good accordance with the minimum potential GH at this site.

An estimate of 29 g of CH_4/cm^2 was made for Site 1040 offshore Costa Rica (Hensen and Wallmann, 2005) applying a geochemical model which considers fluid flow and a different kinetic approach for POC degradation. However, the transfer function does not predict any GH at this site considering a POCar of 2.3 $g/m^2/yr$, because of the low sediment thickness above the décollement (380 m). Indeed at Site 1041 and with a sediment thickness of 750 m within the GHSZ, the function gives an amount of 17 g of CH_4/cm^2, which is still in the expected range.

It should be noted that the function gives lower GHI values than obtained by other methods at high gas flux sites since the ascent of methane with rising fluids and gases is not considered in the model. These additional transport pathways are presently not included in the transfer function because fluid and gas flow are strongly variable in space and time, and hence very difficult to constrain and to generalise. At present, the function predicts the potential of GH formation via biogenic CH_4 formation within the GHSZ, only.

6 Conclusions

In this study we performed a systematic analysis of the key control parameters of biogenic GH formation using the numerical model presented by Wallmann et al. (2006).

The derived transfer function is based on two ubiquitously available parameters, the POC accumulation rate (POCar) and the thickness of the gas hydrate stability zone (GHSZ). Hence, we provide a simple prognostic tool for GH quantification in marine sediments which enables the estimation of GH inventories formed by in situ produced CH_4 without the need of detailed information concerning the geological condition or running complex numerical models. Hence, the extrapolation to regional scales is comparatively simple.

It must be pointed out that the transfer function does not account for effects of fluid advection and methane gas ascent (HGF sites), which means that it will typically predict minimum estimates. However, at low gas flux sites (LGF) sites, which represent the most common setting on a global scale, testing the function has shown that reasonable GH inventories are predicted.

Appendix A

Rate laws and boundary conditions

See Tables A1 and A2.

Acknowledgements. This work has been supported by the DFG financed project HYDRA and the Kiel-based SFB 574 and by the BMBF-financed SUGAR project.

References

Archer, D., Buffett, B., and Brovkin, V.: Ocean methane hydrates as a slow tipping point in the global carbon cycle, P. Natl. Acad. Sci. USA, Special Feature, 106(49), 20596–20601, doi:10.1073/pnas.0800885105, 2008.

Berner, R. A.: The long-term carbon cycle, fossil fuels and atmospheric composition, Nature, 426, 323–326, doi:10.1038/nature02131, 2003.

Berner, R. A.: Early Diagenesis – A Theoretical Approach, Princeton University Press, Princeton, USA, 1980.
Bhatnagar, W., Chapman, G., Dickens, G. R., Dugan, B., and Hirasaki, G. J.: Generalization of gas hydrate distribution and saturation in marine sediments by scaling of thermodynamic and transport processes, Am. J, Sci., 307, 861–900, 2007.
Brown, K. M., Bangs, N. L., Froelich, P. N., and Kvenvolden, K. A.: The nature, distribution and origin of gas hydrate in the Chile triple junction region, Earth Planet. Sc. Lett., 139, 471–483, 1996.
Brown, H. E., Holbrook, W. S., Hornbach, M. J., and Nealon, J.: Slide structure and role of gas hydrate at the northern boundary of the Storegga Slide, offshore Norway, Mar. Geol., 229, 179–186, 2006.
Buffett, B. A. and Archer, D.: Global inventory of methane clathrate: sensitivity to changes in the deep ocean, Earth Planet. Sc. Lett., 227, 185–199, 2004.
Burdige, D. J.: Preservation of Organic Matter in Marine Sediments: Controls, Mechanisms, and an Imbalance in Sediment Organic Carbon Budgets, Chem. Rev., 107, 476–485, 2007.
Chand, S., Minshull, T. A., Gei, D., and Carcione, J. M.: Elastic velocity models for gas-hydrate-bearing sediments – a comparison, Geophys. J. Int., 159, 573–590, 2004.
Chave, A. D. and Cox, C. S.: Controlled Electromagnetic Sources for Measuring Electrical Conductivity beneath the Oceans 1. Forward Problem and Model Study, J. Geophys. Res., 87(B0), 5327–5383, 1982.
Colman A. S. and Holland H. D.: The global diagenetic flux of phosphorus from marine sediments to the oceans: Redox sensitivity and the control of atmospheric oxygen levels. Special Publication, Society for Sedimentary Geology, 66, 53–75, 2000.
D'Hondt, S. L., Jørgensen, B. B., Miller, D. J., Aiello, I. W., Bekins, B., Blake, R., Cragg, B. A., Cypionka, H., Dickens, G. R., Ferdelman, T., Ford, K. H., Gettemy, G. L., Guèrin, G., Hinrichs, K.-U., Holm, N., House, C. H., Inagaki, F., Meister, P., Mitterer, R. M., Naehr, T. H., Niitsuma, S., Parkes, R. J., Schippers, A., Skilbeck, C. G., Smith, D. C., Spivack, A. J., Teske, A., Wiege, J.: Controls on microbial communities in deeply buried sediments, eastern Equatorial Pacific and Peru margin, Sites 1225–1231, Proceedings of the Ocean Drilling Program, Initial Reports, 201, 2003.
Davie, M. K. and Buffett, B. A.: A numerical model for the formation of gas hydrate below the seafloor, J. Geophys. Rev., 106(B1), 497–514, 2001.
Davie M. K. and Buffett, B. A.: Sources of methane for marine gas hydrate: inferences from

a comparison of observations and numerical models, Earth Planet. Sc. Lett., 206, 51–63, 2003.
Dickens, G. R., O'Neil, J. R., Rea, D. K., and Owen, R. M.: Dissociation of oceanic methane hydrate as a cause of the carbon isotope excursion at the end of the Paleocene, Paleoceanogr. Currents, 10(6), 965–971, 1995.
Dickens, G. R., Paull, C. K., Wallace, P., and the ODP Leg 164 Scientific Party: Direct measurement of in situ methane quantities in a large gas-hydrate reservoir, Nature, 385, 426–428, 1997.
Dickens, G. R. and Snyder, G. T.: Interpreting upward methane flux from marine pore water profiles, Fire In The Ice, Winter, Methane Hydrate Newsletter, published by US Department of Energy, Office of Fossil Energy, National Energy Technology Laboratory, 7–10, 2009.
Dobrynin, V., Korotajev, Y., and Plyuschev, D.: Gas Hydrates: A Possible Energy Resource, in: Long-Term Energy Resources, edited by: Meyer, R. and Olson, J., Boston, MA, Pitman, 727–729, 1981.
Egeberg, P. K. and Dickens, G. R.: Thermodynamic and pore water halogen constraints in gas hydrate distribution at ODP Site 997 (Blake Ridge), Chem. Geol., 153, 53–79, 1999.
Ersland, G., Husebø, J., Graue, A., and Kvamme, B.: Transport and storage of CO2 in natural gas hydrate reservoirs, Energy Procedia, 1, 3477–3484, 2009.
Ford, K. H., Naehr, T. H., Skilbeck, C. G., and the Leg 201 Scientific Party: The use of infrared thermal imaging to identify gas hydrate in sediment cores, in: Proceedings of the Ocean Drilling Program, edited by: D'Hondt, S. L., Jørgensen, B. B., Miller, D. J ., et al., Initial Reports, 201, 1–20, 2003.
Haeckel, M., Suess, E., Wallmann, K., and Rickert, D.: Rising methane gas bubbles form massive hydrate layers at the seafloor, Geochim. Cosmochim. Ac., 68(21), 4335–4345, 2004.
Heeschen, K. U., Hohnberg, H. J ., Haeckel, M., Abegg, F., Drews, M., and Bohrmann, G.: In situ hydrocarbon concentration from pressurised cores in surface sediments, Northern Gulf of Mexico, Mar. Chem., 107, 498–515, 2007.
Hensen, C. and Wallmann, K.: Methane formation at Costa Rica continental margin - constraints for gas hydrate inventories and cross-décollement fluid flow, Earth Planet. Sc. Lett., 236, 41–60, 2005.
Hesse, R.: Pore water anomalies of submarine gas-hydrate zones as tool to assess hydrate abundance and distribution in the subsurface. What have we learned in the past decade?, Earth Sci. Rev., 61, 149–179, 2003.

Hustoft, S., Bunz, S., Mienert, J., and Chand, S.: Gas hydrate reservoir and active methane-venting province in sediments on <20 Ma young oceanic crust in the Fram Strait, offshore NW-Svalbard, Earth Planet. Sc. Lett., 284(1–2), 12–24, doi:10.1016/j.epsl.2009.03.038, 2009.

Hyndman, R. D., Yuan, T., and Moran, T. Y.: The concentration of deep sea gas hydrates from downhole electrical resistivity logs and laboratory data, Earth Planet. Sc. Lett., 172, 167–177, 1999.

Kastner, M., Torres, M., Solomon, E., and Spivack, A. J.: Marine Pore Fluid Profiles of Dissolved Sulfate; Do They Reflect In Situ Methane Fluxes?, Fire In The Ice, Summer, Methane Hydrate Newsletter, published by US Department of Energy, Office of Fossil Energy, National Energy Technology Laboratory, 6–8, 2008a.

Kastner, M., Spivack, A. J., Torres, M., Solomon, E., Borole, D. V., Robertson, G., and Das, H. C.: Gas hydrates in three Indian ocean regions, a comparative study of occurrence and subsurface hydrology, Proceedings of the 6th International Conference on Gas Hydrates (ICGH 2008), Vancouver, British Columbia, Canada, 2008b.

Kennett, J. P., Cannariato, K. G., Hendy, I. L., and Behl, R. J.: Methane Hydrates in Quaternary Climate Change, The Clathrate Gun Hypothesis, American Geophysical Union, Washington, DC, 216 pp., 2003.

Kimura, G., Silver, E., Blum, P., et al.: Proceedings of the Ocean drilling Programm, Initial Reports, 170, College Station, TX, 458 pp., 1997.

Klauda, J. B. and Sandler, S. I.: Global Distribution of Methane Hydrate in Ocean Sediment, Energ. Fuel, 19, 459–470, 2005.

Kvenvolden, K. A.: Methane hydrates - a major reservoir of carbon in the shallow geosphere?, Chem. Geol., 71, 41–51, 1988.

Liu, X. and Flemmings, P. B.: Dynamic multiphase flow model of hydrate formation in marine sediments, J. Geophys. Rev., 112, B03101, doi:10.1029/2005JB004227, 2007.

Malinverno, A., Kastner, M., Torres, M. E., and Wortmann, U. G.: Gas hydrate occurrence from pore water chlorinity and downhole logs in a transect across the northern Cascadia margin (Integrated Ocean Drilling Program Expedition 311), J. Geophys. Res., 113, B08103, doi:10.1029/2008JB005702, 2008.

Middelburg, J.: A simple rate model for organic matter decomposition in marine sediments, Geochim. Cosmochim. Ac., 53, 1577–1581, 1989.

Milkov, A. V.: Global estimates of hydrate-bound gas in marine sediments: how much is really

out there?, Earth Sci. Rev., 66, 183–197, 2004.
Milkov, A. V.: Molecular and stable isotope compositions of natural gas hydrates: A revised global dataset and basic interpretations in the context of geological settings, Org. Geochem., 36(5), 681–702, 2005.
Mix, A. C., Tiedemann, R., Blum, P., et al.: Proceedings of the Ocean Drilling Program, Initial Reports, 202, 2003.
Moridis, G. J., Collett, T. S., Dallimore, S. R., Satoh, T., Hancock, S., and Weatherill, B.: Numerical studies of gas production from several CH_4 hydrate zones at the Mallik site, Mackenzie Delta, Canada, J. Petrol. Sci. Eng., 43, 219–238, 2004.
Paull, C. K., Matsumoto, R., Wallace, P. J., et al.: Proceedings of the Ocean Drilling Program, Initial Reports, Vol. 164, 1996.
Paull, C. K., Matsumoto, R., Wallace, P. J., and Dillon, W. P. (eds.): Proc. ODP, Sci. Results, 164: College Station, TX (Ocean Drilling Program), 2000.
Pollack, H. N., Hurter, S. J., and Johnson, J. R.: Heat Flow from the Earth's Interior: Analysis of the Global Data Set, Rev. Geophys., 31(3), 267–280, 1993.
Riedel, M., Willoughby, E. C., Chen, M. A., He, T., Novosel, I., Schwalenberg, K., Hyndman, R. D., Spence, G. D., Chapman, N. R., and Edwards, R. N.: Gas hydrate on the northern Cascadia margin: regional geophysics and structural framework, edited by: Riedel, M., Collett, T. S., Malone, M. J., and the Expedition 311 Scientists, Proc. IODP, 311, Washington, DC (Integrated Ocean Drilling Program Management International, Inc.), doi:10.2204/iodp.proc.311.109.2006, 2006.
Schwalenberg, K., Willoughby, E., Mir, R., and Nigel Edwards, R.: Marine gas hydrate electromagnetic signatures in Cascadia and their correlation with seismic blank zones, First Break, 23, Special Topic, Petroleum Geology, 57–63, 2005.
Seiter, K., Hensen, C., Schröte, J., and Zabel, M.: Organic carbon content in surface sediments – defining regional provinces, Global Biogeochem. Cy, GB1010, 1–26, 2004.
Sloan, E. D. and Koh, C. A.: Clathrate hydrates of natural gases, Chapter Hydrate Dissociation, in Chemical Industries/119, 3.edit., CRC Press, New York, USA, 752 pp., 2007.
Soloviev, V. A.: Global estimation of gas content in submarine gas hydrate accumulations, Russ. Geol. Geophys., 43, 609–624, 2002.
Suess, E., von Huene, R., Emeis, K.-C., and the Scientific Shipboard Party: Proceedings of the Ocean Drilling Program, Initial Reports, 112, doi:10.2973/odp.proc.ir.112.102.1988, 1988.
Tishchenko, P., Hensen, C., Wallmann, K., and Wong, C. S.: Calculation of the stability and

solubility of methane hydrate in seawater, Chem. Geol., 219, 37–52, 2005.
Torres, M. E., Wallmann, K., Tréhu, A. M., Bohrmann, G., Borowski, W. S., and Tomaru, H.: Gas hydrate growth, methane transport, and chloride enrichment at the southern summit of Hydrate Ridge, Cascadia margin off Oregon, Earth Planet. Sc. Lett., 226, 225–241, 2004.
Torres, M. E., Tréhu, A. M., Cespedes, N., Kastner, M., Wortmann, U. G., Kim, J. H., Long, P., Malinverno, A., Pohlman, J. W., Riedel, M., and Collett, T.: Methane hydrate formation in turbidite sediments of northern Cascadia, IODPExpedition 311, Earth Planet. Sc. Lett., 271, 170–180, 2008.
Tréhu, A. M., Torres, M. E., Long, P. E., Torres, M. E., Bohrmann, G., Rack, F. R , Collet, T. S., Goldberg, D. S. , Milkov, A. V., Riedel, M., Schultheiss, P., Bangs, N. L., Barr, S. R., Borowski, W. S., Claypool, G. E., Delwiche, M. E., Dickens, G. R., Gracia, E., Guerin, G., Holland, M. , Johnson, J. E., Lee, Y.-J., Liu, C.-S., Su, X., Teichert, B., Tomaru, H., Vanneste, M., Watanabe, M., and Weinberger, J. L.: Three-dimensional distribution of gas hydrate beneath southern Hydrate Ridge: constraints from ODP Leg 204, Earth Planet. Sc. Lett., 222, 845–862, 2004.
Tromp, T. K., Van Cappellen, P., and Key, R. M.: A global model for the early diagenesis of organic carbon and organic phosphorus in marine sediments, Geochim. Cosmochim. Ac., 59(7), 1259–1284, 1995.
Uchida, T., Lu, H., Tomaru, H. and the MITI Nankai Trough Shipboard Scientists: Subsurface Occurrence of Natural Gas Hydrate in the Nankai Trough Area: Implication for Gas Hydrate Concentration, in: Resource Geologym., 54, 35–44, doi:10.1111/j.1751-3928.2004.tb00185.x, 2004.
Wallmann, K., Aloisi, G. Haeckel, M., Obzhirov, A., Pavlova, G., and Tishchenko, P.: Kinetics of organic matter degradation, microbial methane generation, and gas hydrate formation in anoxic marine sediments, Geochim. Cosmochim. Ac., 70, 3905–3927, 2006.
Westbrook, G. K., Chand, S., Rossi, G., Long, C., Bünz, S., Camerlenghi, A., Caricione, J. M., Dean, S., Foucher, J.-P., Flueh, E., Gei, D., Haacke, R. R., Madrussane, G., Mienert, J., Minshull, T. A., Nouzé, H., Peacock, S., Reston, T. J., Vanneste, M., and Zillmer, M.: Estimation of gas hydrate concentration from multi-component seismic data at sites on the continental margins of NW Svalbard and the Storegga region of Norway, Mar. Petrol. Geol., 25, 744–758, 2008.
Westbrook, G. K., Carson, B., Musgrave, R. J., et al.: Proceedings of the Ocean Drilling Program, Initial Reports, 146, 1994.

Xu, W. and Germanovich, L. N.: Excess pore pressure resulting from methane hydrate dissociation in marine sediments: A theoretical approach, J. Geophys. Res., 111, BO1104, doi:10.1029/2004JB003600, 2006.

Yuan, T., Hyndman, R. D., Spence, G. D., and Desmons, B.: Seismic velocity increase and deep-sea gas hydrate concentration above a bottom-simulating reflector on the nothern Cascadia continental slope, J. Geophys. Res., B101, 13655–13671, 1996.

Zhou, X., Fan, S., Liang, D., and Du, J.: Replacement of methane from quartz sandbearing hydrate with carbon dioxide-in-water emulsion, Energ. Fuel, 22(3), 1759–1764, 2008.

Table 1. Parameters, constants and coefficients of the modelled ODP Sites 1041 (Costa Rica), 685 and 1230 (Peru), 1233 (Chile), 1014 (California), 995 (Blake Ridge), and 1084 (Namibia). The varying values for the different model runs (constant POC input, varying POC input and fluid flow) are listed as a, b, and c. The porosity is calculated after Berner (1980) with the porosity at the surface ($P0$), at the lower boundary (Pf) and the coefficient for the decrease of porosity px.

Region		Costa Rica	Peru		Chile	California	Blake Ridge	Namibia
ODP Site		1041	1230	685	1233	1014	995	1084
Water depth [m]		3305	5086	5070	838	1165	2779	1992
Seafloor temperature [°C]		1.9	1.7	1.4	5	4.1	3.6	3.5
Thermal gradient [°/km]		21.6	34.3	42	45	58	36.9	48
Sedimentation rate [cm/kyr]		13.1	100	14.7	110	79	40	24
Sediment thickness [m]		750	270	620	120	500	900	620
N/C		16/160	16/106	16/106	16/145	16/170	16/140	16/170
NH_4 adsorption coefficient (K_{NH_4})								
[cm^3 pore water/g solids]	a/b/c	1.3/1.9/–	0.1/–/–	0.1/–/0.1	0.8/0.7/0.1	0.01/–/–	0.3/0.6/–	0.1/–/0.1
POC [wt.%]	a/b/c	1.6/1.2–3.0/–	2.8/–/–	3.2/–/3.2	1.2/1.1–2.1/0.9–2.1	5/–/–	1.6/0.25–1.9/–	8/8
Initial age of POC								
(age_{init}) [kyr]	a/b/c	100/100/–	40/–/–	45/–/20	0.8/1.5/3	50/–/–	180/25/–	43/–/43
POC Inhibition constant								
(K_C) [mmol/l]	a/b/c	43/44/–	45/–/–	43/–/45	50/45/45	25/–/–	45/45/–	45/–/45
Fluid Flow [mm/yr]	c	–	–	0.16	1.1	–	–	0.18
Porosity $P0$		0.7	0.76	0.76	0.77	0.8	0.76	0.85
Pf		0.52	0.65	0.56	0.62	0.6	0.52	0.7
$1/px$		20 000	5000	17 000	1800	4000	17 000	4000

Table 2. Input parameters and boundary conditions for the standard model using average values of all specific ODP models. The range of parameter values used for the sensitivity analysis are also shown.

	Standard model (average of ODP models)	Sensitivity analysis
Thermal gradient [°/km]	44.2	10–65
Seafloor temperature [°C]	3.1	1–6
Water depth [m]	2516	500–5500
GHSZ [m]	450	50–2000
POC accumulation rate [g/m^2/yr]	4.3	0.7–40
– POC input [wt.%]	2.3	1.2–3.1
– Sedimentation rate [cm/kyr]	32	9.5–200
Initial age of POC [kyr]	43.7	43.7
Inhibition constant of POC degradation [mmol/l]	43	43

Table 3. Comparison of the GH amounts of the ODP sites calculated in the different model runs: **(a)** constant POC input, **(b)** varying POC input, **(c)** time-dependent POC input and advective fluid flow, with the transfer function, using the input data of the ODP models.

ODP Site/model		GHI (numerical model) [g CH_4/cm^2]	GHI (transfer function) [g CH_4/cm^2]
1041	a)	6.2	16.9
	b)	7.3	16.9
1230	a)	10	2.2
685	a)	26.4	25.2
	c)	66	25.2
1233	a)	0	0
	b)	0	0.12
	c)	0	0
1014	a)	0.55	0
995	a)	0	15
	b)	3.0	15
1084	a)	23.7	5.0
	c)	39.7	5.0

Table 4. Comparison of the GHI amount calculated with the transfer function to other published results obtained from several approaches, such as seismic velocity calculations, chlorinity, resistivity log or a combination of several of these methods. Other results obtained by numerical modelling are also shown.

Setting	GHI [g CH_4/cm^2] transf. funct.	Literature	Approach	Reference
Blake Ridge				
Sites 997/995	7.8/15	48–97	Several approaches	Paull et al., 2000
Site 997	7.8	26.2	Model	Davie and Buffett, 2003
Site 997	7.8	5.1	Model	Wallmann et al., 2006
Hydrate Ridge				
Sites 1244–1248	0	< 19	Several approaches	Tréhu et al., 2004
Site 889	0	13	Model	Davie and Buffett, 2003
Northern Cascadia				
Sites 1325–1327	0–0.5	0.4–0.8	Model	Malinverno et al., 2008
Sites 1325-1327	0–0.5	57	Several approaches	Torres et al., 2008
Costa Rica				
Site 1040	0	29	Model	Hensen and Wallmann, 2005
Site 1041	17			
Chile				
Site 1233	0			
Site 859	10	< 17.5	Seismic velocity	Brown et al., 1996
Site 859	10	< 40	Chlorinity	Brown et al., 1996
India				
Site 10 (NGHP)	5.80	8–495	Chlorinity	Kastner et al., 2008b

Table A1. Summary of the main rate laws.

Process	Rate law
POC degradation	$R_{POC} = \frac{K_C}{C(CH_4)+C(DIC)+K_C} \cdot \left(0.16 \cdot (age_{init} + age_{sed})^{-0.95}\right) \cdot C(POC)$
Methanogenesis	$R_{CH_4} = 0.5 \cdot \frac{K_{SO_4}}{K_{SO_4}+C(SO_4)} \cdot R_{POC}$
Anaerobic oxidation of methane (AOM)	$R_{AOM} = k_{AOM} \cdot C(CH_4) \cdot C(SO_4)$
Sulphate reduction	$R_{SO_4} = 0.5 \cdot \frac{C(SO_4)}{K_{SO_4}+C(SO_4)} \cdot R_{POC}$
GH formation	$R_{GH-form} = k_{GH} \cdot (C(CH_4)/\text{Stability} - 1)$
GH dissociation	$R_{GH-diss} = k_{DGH} \cdot (\text{Stability}/C(CH_4) - 1) \cdot C(GH)$
FG formation	$R_{FG-form} = k_{FG} \cdot (C(CH_4)/\text{Solubility} - 1)$
FG dissolution	$R_{FG-diss} = k_{DFG} \cdot (\text{Solubility}/C(CH_4) - 1) \cdot C(FG)$
PON degradation	$R_{PON} = R_{POC} \cdot (N/C)$
Ammonium adsorption	$R_{NH_4-ads} = k_{ads} \cdot (1 - C(NH_{4_{-ads}})/C(NH_4)/K_{NH_4})$

BGD
7, 1057–1099, 2010

Table A2. Boundary conditions and constants used for the ODP model. Nomenclature after Wallmann et al. (2006).

Parameter/Coefficient	Value
Kinetic constant for AOM (k_{AOM})1/(mmol/cm^3/yr)	1
Kinetic constant for NH_4 adsorption (k_{ads}) [mmol/cm^3/yr]	0.0001
Density of dry solids [g/cm^3]	2.5
Monod constant for SO_4 reduction (k_{SO_4}) [mmol/cm^3]	0.001
Kinetic constant for GH precipitation (k_{GH}) [wt.%/yr]	0.005
Kinetic constant for GH dissolution (k_{DGH}) [1/yr]	0.02
Kinetic constant for FG precipitation (k_{FG}) [vol.%/yr]	0.5
Kinetic constant for FG dissolution (k_{DFG}) [1/yr]	0.5
SO_4 concentration upper/lower boundary [mmol/l]	28/0
CH_4 concentration upper boundary [mmol/l]	0
NH_4 concentration upper boundary [mmol/l]	0

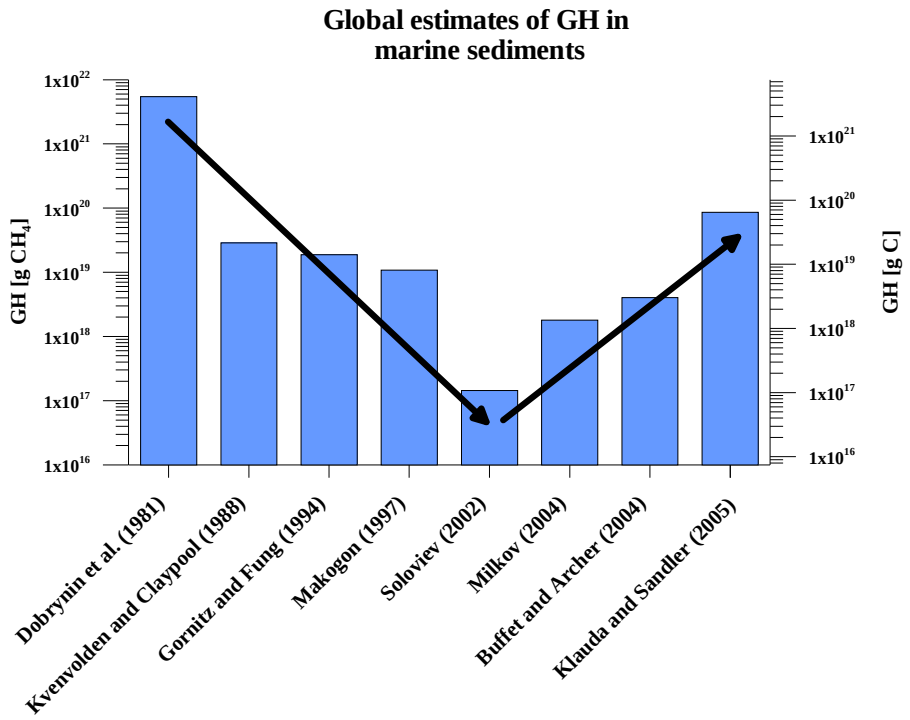

Fig. 1. Selected estimates of global GH inventories since the early 1980's. The quantities range over 5 orders of magnitude from 10^{17} to 10^{22} g of CH_4. At present, an inventory of about 4×10^{18} g of CH_4 (3000 Gt C) estimated by Buffett and Archer (2004) seems to be the most likely scenario.

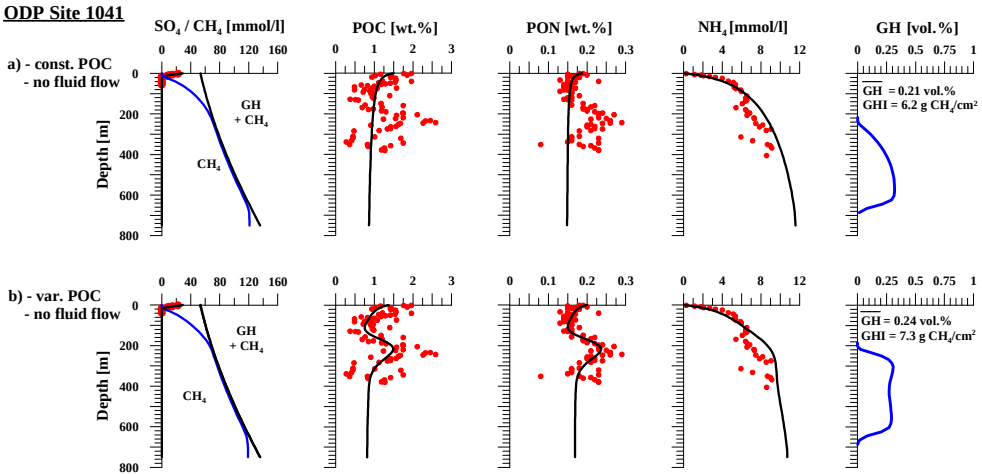

Fig. 2. Model results for ODP Site 1041 off Costa Rica for two different model runs: **(a)** constant POC input, and **(b)** varying POC input over time. In the GH plot the average GH concentration (in % of the pore space) and the integrated GHI amount (in g CH_4/cm^2) are given.

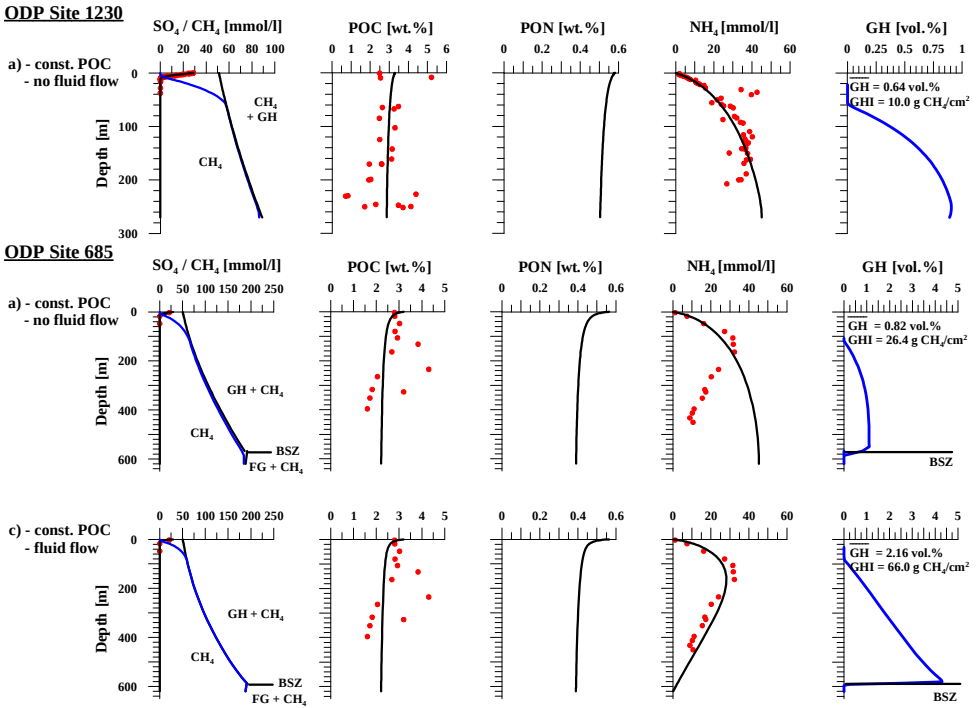

Fig. 3. Model results for ODP Sites 1230 and 685 off Peru for two different model runs: **(a)** constant POC input, and **(c)** constant POC input with advective fluid flow. In the GH plot the average GH concentration (in % of the pore space) and the integrated GHI amount (in g CH_4/cm^2) are given.

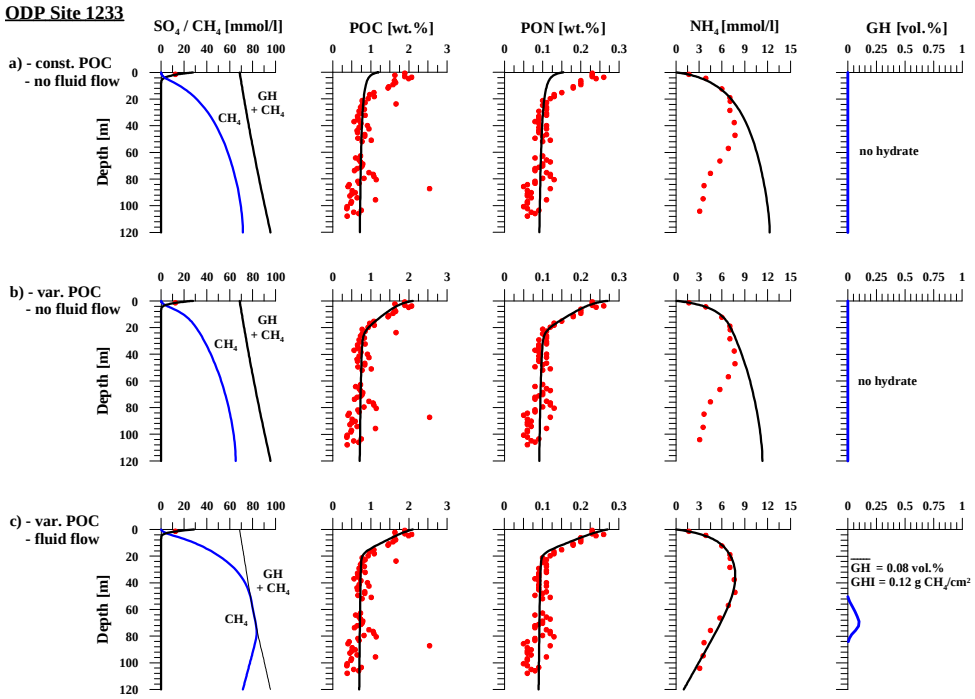

Fig. 4. Model results for ODP Sites 1233 off Chile for three different model runs: **(a)** constant POC input, **(b)** varying POC input, and **(c)** varying POC input combined with advective fluid flow. In the GH plot the average GH concentration (in % of the pore space) and the integrated GHI amount (in g CH_4/cm^2) are given.

BGD
7, 1057–1099, 2010

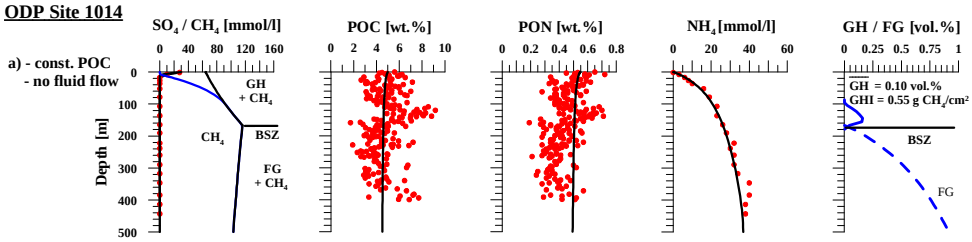

Fig. 5. Model results for ODP Site 1014 off California with **(a)** constant POC input. The dotted line indicates the free gas (FG) contents below the base of the GHSZ (BSZ) in % of the pore space. In the GH plot the average GH concentration (in % of the pore space) and the integrated GHI amount (in g CH_4/cm^2) are given.

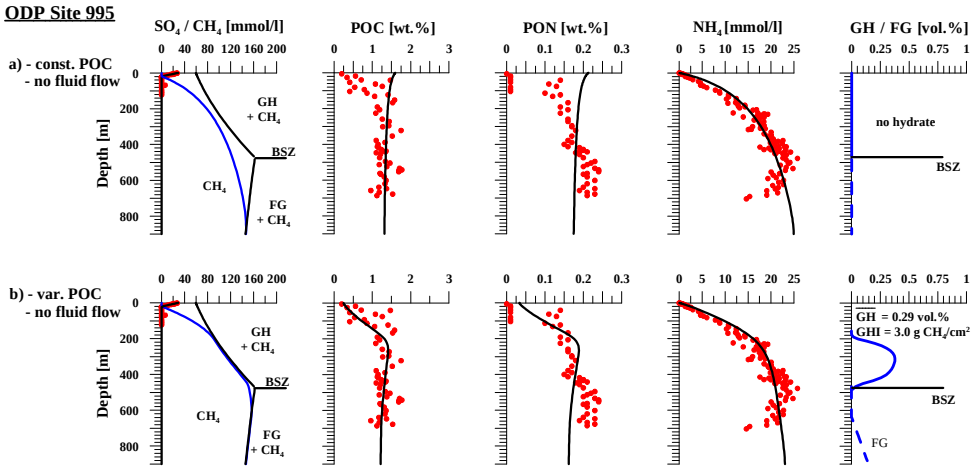

Fig. 6. Model results for ODP Site 995 at Blake Ridge for two different model runs: **(a)** constant POC input, and **(b)** time varying POC input. The dotted line indicates the free gas (FG) contents below the base of the GHSZ (BSZ) in % of the pore space. In the GH plot the average GH concentration (in % of the pore space) and the integrated GHI amount (in g CH_4/cm^2) are given.

BGD
7, 1057–1099, 2010

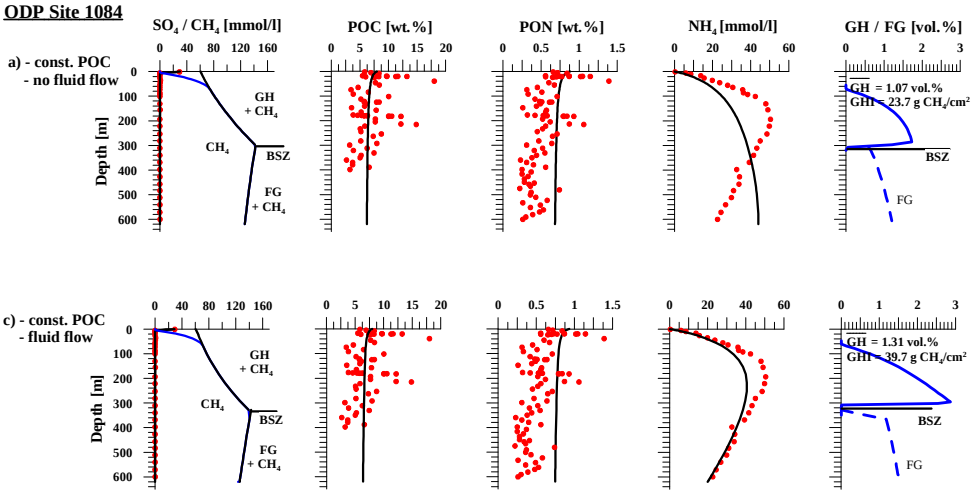

Fig. 7. Model results for ODP Site 1084 off Namibia for two different model runs: **(a)** constant POC input, and **(c)** constant POC input combined with advective fluid flow. The dotted line indicates the free gas (FG) contents below the base of the GHSZ (BSZ) in % of the pore space. In the GH plot the average GH concentration (in % of the pore space) and the integrated GHI amount (in g CH_4/cm^2) are given.

BGD
7, 1057–1099, 2010

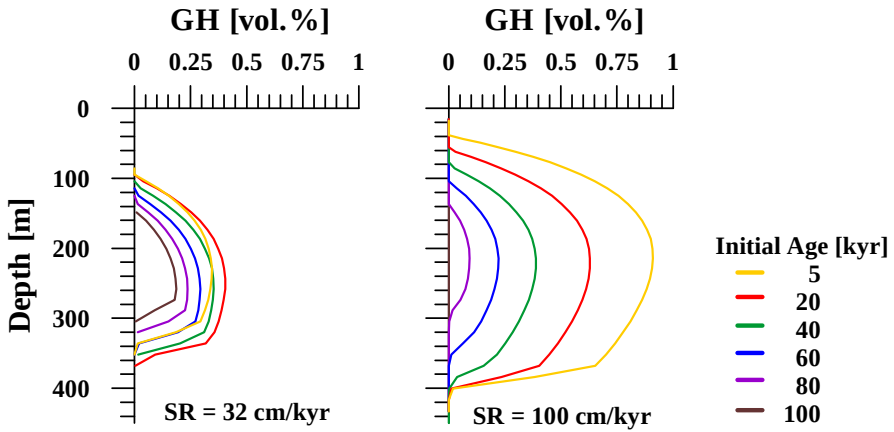

Fig. 8. Effect of the initial POC age on the accumulation of gas hydrates in marine sediments.

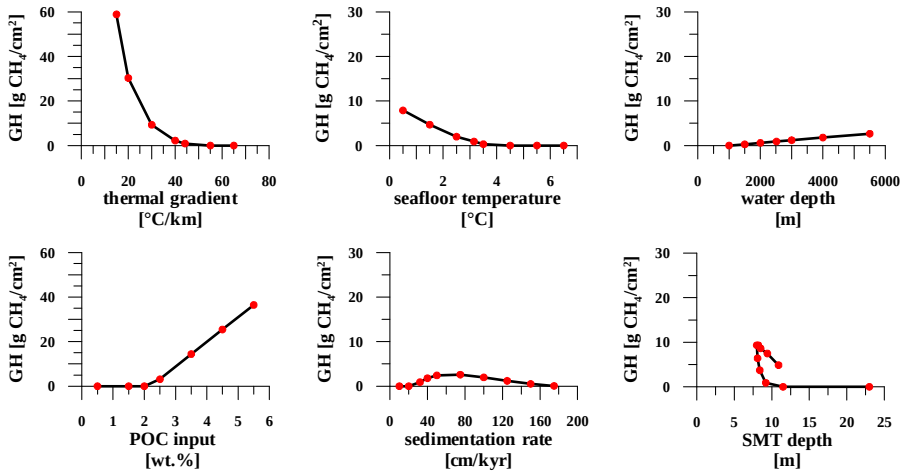

Fig. 9. Sensitivity analysis of the standard model: For each model run (red dots) only one input parameter was varied. Additionally, the resulting output parameter SO_4-CH_4-transition depth (SMT) is shown.

BGD
7, 1057–1099, 2010

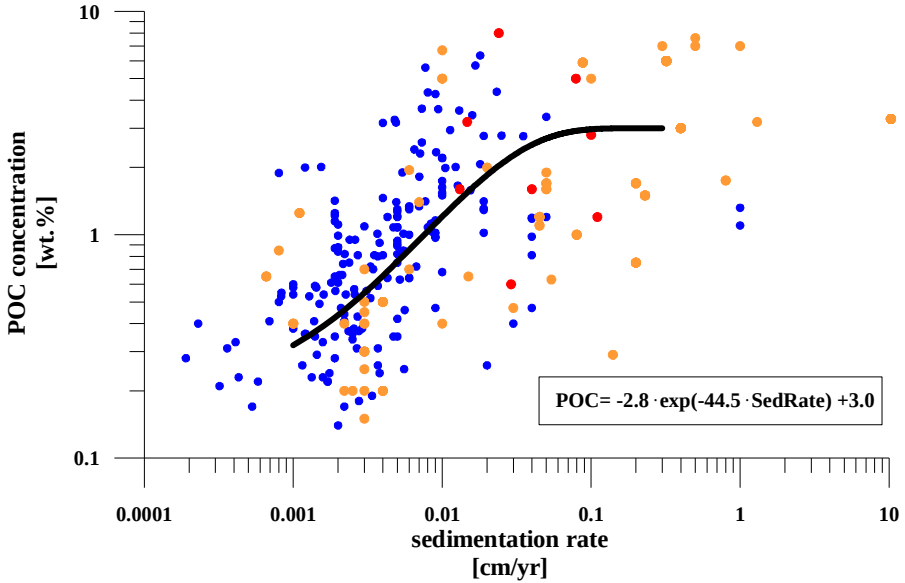

Fig. 10. POC concentrations vs. sedimentation rates after Seiter et al. (2004) (blues dots), Colman and Holland (2000) (yellow dots), and the ODP Sites used in this study (red dots) (references are listed in the text). The black line indicates the function derived from the sensitivity analysis.

BGD
7, 1057–1099, 2010

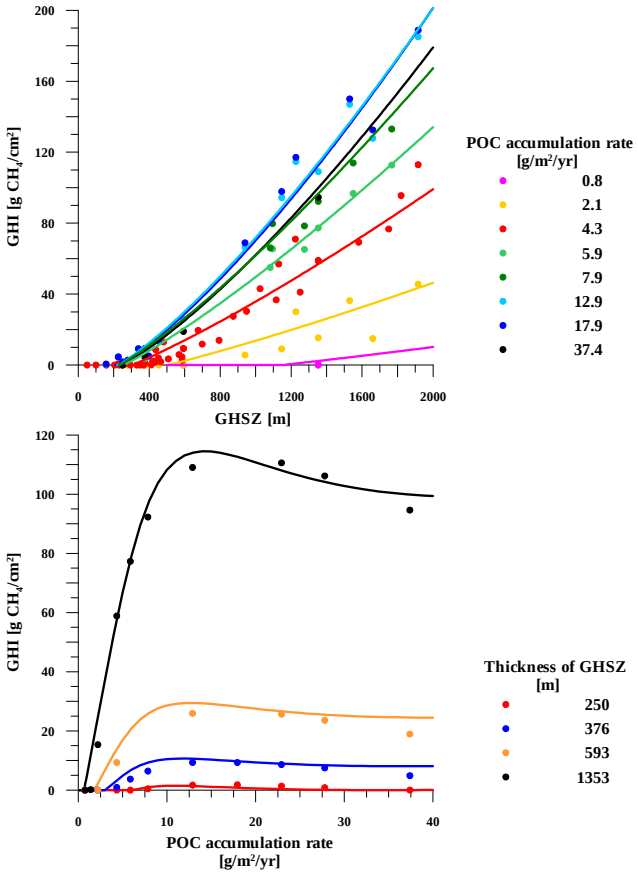

Fig. 11. Parameter analysis of the two key control parameters POCar and GHSZ: **(a)** relation of GHSZ and GH accumulation for varying POCar. **(b)** relation of POCar and GH accumulation for varying GHSZ.

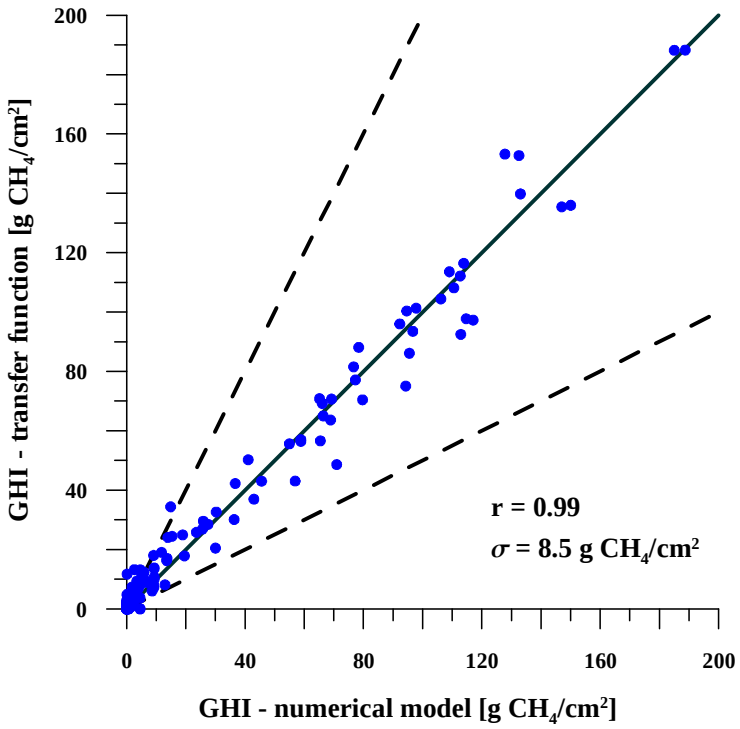

Fig. 12. Crossplot of the GH masses estimated by the transfer function and the numerical models (sensitivity- and parameter analyses). The solid line shows the 1:1 correlation, the dotted lines the 50% deviation interval. The standard deviation σ and the correlation coefficient r are indicated.

BGD
7, 1057–1099, 2010